ISSN 0027-1349, Moscow University Physics Bulletin, 2020, Vol. 75, No. 6, pp. 638–644. © Allerton Press, Inc., 2020.

BIOPHYSICS AND MEDICAL PHYSICS

Monte Carlo Simulation Method Highlighting on the Electron Beam Irradiation on the Structure of SARS-CoV-2

Adil Bardane[1]*, Jaouad Tajmouati[1], Abdelmajid Maghnouj[1], and Ahmed Dadouch[1]

[1] *LISTA Laboratory, Physics Department, Faculty of Sciences Dhar El-Mahraz, Sidi Mohamed Ben Abdellah University, Fez, Morocco*

Received May 23, 2020; revised August 24, 2020; accepted November 3, 2020

Abstract—The outbreak of SARS-CoV-2 resulted in more than 11 000 000 infections and over 530 000 deaths. Coronavirus (S) spike glycoproteins promote entry into cells and are the main target of antibodies. We studied the effect of electron beams on the SARS CoV-2 glycoprotein and also on RNA using Monte Carlo simulation. We demonstrated that S-SARS CoV peak glycoproteins damaged by irradiation electrons corresponding to an energy loss of approximately 1.2 keV with a damage rate of the efficiency that can be as high as 68%.

Keywords: SARS-CoV-2, Monte Carlo, electron beam irradiation, RNA, spike glycoproteins

DOI: 10.3103/S0027134920060041

1. INTRODUCTION

Currently, because of the new threat of SARS VOC-2 in the world, many researchers and companies are trying to find effective results to save humanity. Until the beginning of the second millennium, virologists knew that only two viruses of this family infect humans (HCoV-229E and HCoV-OC43).

In 2003, the SARS virus appeared in Hong Kong and China, and in 2004 a new strain called NL63 was discovered. In 2005, a research group at the University of Hong Kong recorded the discovery of a fifth strain called HKU1 [1].

In June 2012, the first patient died of a Coronavirus infection, different from the previously known types, and the infection was in Saudi Arabia. Initially, the virus was given many names and it was recently agreed to name it Coronavirus, which causes MERS-CoV [2].

In December 2019, pneumonia was reported in Wuhan, China. Officially named 2019-nCoV by the World Health Organization. As of July 2, 2020, 516 738 confirmed deaths, and more than 10 717 158 confirmed cases had been reported. The Wuhan strain has been defined as a new strain of group 2B corona beta virus with a genetic similarity of approximately 70% to the SARS virus. The virus was believed to be the root of the snake, but many prominent researchers disagreed with this belief. The virus is 96% similar to the corona bat virus, so it is widely believed to be of bat origin [3]. Forcing millions of people to isolate themselves in their homes to avoid infection, soapy water is the first line of defense to attack the virus on surfaces, and ethanol has been proven to kill coronaviruses in less than 30 s. In industry, radiation and particle radiation can be used to kill bacteria and viruses quickly and effectively [4].

Recent studies have shown several different viruses and how long they stay on surfaces, including SARS-CoV-2 which causes COVID-19, and it appears that the duration of the virus varies depending on the type of surface. Through studies, it has been established that the virus stayed up to nine days on stainless steel (rustproofing) surfaces, while it stayed up to one day on paper and cardboard. Compared to the ultraviolet disinfection method for killing the virus, electron beam radiation with high keV energy can only concentrate the loss of energy more effectively on surface viruses. Although much research and studies have been carried out on electron beam radiation of the virus worldwide [5], this is still not enough. How the radioactive electron interacts with the new coronavirus (COVID-19) remains uncertain. This is due to the difficulty of conducting the electron radiation experiment on the new coronavirus at the present stage and remains a major concern. Theoretical research by numerical simulation is an important means of explaining this phenomenon [6].

In this work, first, we studied the characteristics and results of the interaction of the radioactive

*E-mail: adil.bardane@usmba.ac.ma

beam with the new Coronavirus (COVID-19) using the Monte Carlo numerical simulation. Approved the physical model of COVID-19 granted by Protein Data Bank. The interactions are calculated, including the elastic and inelastic scattering between the radioactive electrons and all the protein layers of the virus.

In the second part, we present a method for calculating damage to COVID-19 using a more realistic description of the virus molecules. The strategy is indeed to combine the atomistic description of the Coronavirus molecules with the energy deposits calculated with Geant4-DNA.

Through this literature review, there is no doubt that the problem of irradiation of the structure of COVID 19 is widely studied. Despite this, to the author's knowledge, the calculation of the number of single and double-strand breaks has not yet been studied.

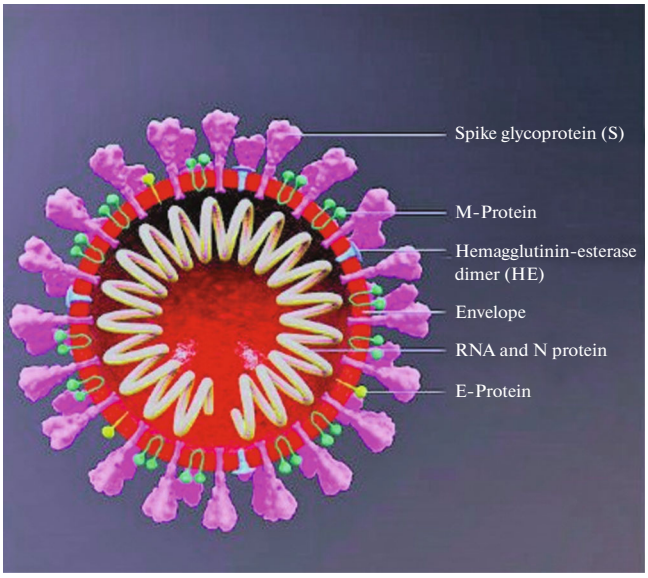

Fig. 1. COVID-19 structure.

2. MATERIALS AND METHODS

2.1. Virus Structure Model

As the new coronavirus (COVID-19) has many types of proteins of surrounding function [7], for the feasibility of the calculation, we choose here three types of proteins mainly during the construction of the physical model with a reasonable simplification. Like other coronaviruses discovered [8], such as SARS, MERS, the new coronavirus (COVID-19) is first surrounded by a few scattered spike glycoproteins, as shown in Fig. 1 [6], and then under the spike glycoproteins there is more than one layer of envelope proteins Table 1. Although in this area there is still a fraction of haemagglutinin which helps to fuse viruses to cells [9], in our physical model we choose as representing the envelope proteins mainly. Inside the new coronavirus, the nucleocapsid tightly attaches RNA, both wander inside the virus with an empty space. Given the complex structure of RNA space and the randomness of RNA movement, we can therefore treat them in our physical model as the nucleocapsid surrounds the RNA in a uniform region. The constituent elements including the spike glycoproteins, the envelope, the nucleocapsid and the RNA are represented by Z1, Z2, Z3, and Z4, respectively. As reported by the Centers for Disease Control and Prevention (CDC), COVID-19 is a large virus with a diameter of approximately 120 nm [10]. Thus, in this study, the thickness of Z1, Z2, and Z3 is fixed at 20, 20, and 10 nm respectively, and the (Z4) RNA is in the 25 nm radius [8].

In our studies, we used a PDB file, representing the N-terminal RNA structure of the phosphoprotein of the SARS-CoV-2 nucleocapsid [11].

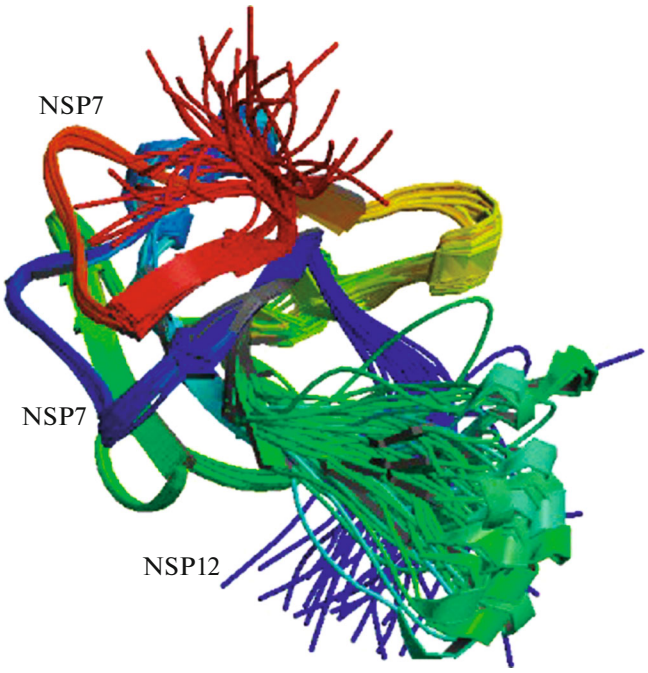

Fig. 2. Visualization of RNA SARS-CoV-19 PDB files.NSP: non-structural proteins.

2.2. Physics

The electron interacts with atomic electrons or nuclei through Coulomb interactions. Electrons can undergo elastic or inelastic interactions. During an elastic interaction, the incident electron is deflected without losing energy (diffusion). During an inelastic interaction, the incident electron is deflected out of its path and transfers part of its kinetic energy

Table 1. Statistical data of proteins from NCBI

	Spike proteine (S)	Enveloppe proteine	N-proteine	RNA
Average molecular weight	128.89	131.19	124.42	126.46
Average molecular formula	$C_{4.95}H_{9.67}O_{2.49}$ $N_{1.2}S_{0.04}$	$C_{5.23}H_{10.2}O_{2.35}$ $N_{1.25}S_{0.03}$	$C_{4.61}H_{9.29}O_{2.45}$ $N_{1.3}S_{0.02}$	$C_{4.5}H_{4.68}O_{1.02}N_{3.67}$

Table 2. The most commonly used names in PDB files

Denomination	Description
HEADER, TITLE, and AUTHOR	Information on the researchers who defined the structure; any other general type of information
ATOM	Coordinates (X, Y, Z) of the atoms, expressed in Angstrm, the chain identifier, and the residue number (the group of atoms corresponding to the nucleotide in the case of DNA)
HETATM	Coordinates (X, Y, Z) of the atoms, expressed in Angstrm
TER	End of a residue chain
HELIX	Location and type of propellers
SHEET	Location, direction in relation to the previous strand

to an atomic electron or in the form of braking radiation ("Bremsstrahlung"). Standard models for electrons in Geant4 include the ionization process, Bremsstrahlung, multiple scattering, and single scattering.

2.2.1. Ionization. The energy loss (stopping power) for ionization in the Standard model is based on the Berger–Seltzer formula derived from Bethe–Bloch theory. The energy loss of an electron with kinetic energy E below the threshold of secondary particles T_{cut} is given by the following formula:

$$\left(\frac{dE}{dx}\right)_{T<T_{\text{cut}}} = 2\pi r_e^2 mc^2 n_{el} \times \frac{1}{\beta^2}\left[\ln\frac{2(\gamma+1)}{(\frac{I}{mc^2})^2} + F \pm (\tau, \tau_{up}) - \delta\right] \quad (1)$$

such as:
dx: distance traveled,
r_e: electron radius,
mc^2: mass energy of the electron,
n_{el}: densit electronique,

```
HEADER    VIRAL PROTEIN                          16-MAR-20   6M71
TITLE     SARS-COV-2 RNA-DEPENDENT RNA POLYMERASE IN COMPLEX WITH COFACTORS
COMPND    MOL_ID: 1;
COMPND   2 MOLECULE: SARS-COV-2 NSP12;
      ...
HELIX   24 AC6 SER A  520  LYS A  532  1                                  13
HELIX   25 AC7 SER A  561  ALA A  581  1                                  21
HELIX   26 AC8 GLY A  596  TYR A  606  1                                  11
      ...
ATOM   2207  CD1 LEU A 329     120.506 149.546 127.810  1.00 53.73           C
ATOM   2208  CD2 LEU A 329     122.200 148.386 129.231  1.00 53.73           C
ATOM   2209  N   VAL A 330     119.772 150.109 133.554  1.00 59.40           N
      ...
SHEET    4 AA7 4 THR A 801  GLU A 802 -1  O  GLU A 802   N  LEU A 614
SHEET    1 AA8 2 HIS A 816  LYS A 821  0
SHEET    2 AA8 2 TYR A 826  TYR A 831 -1  O  LEU A 829   N  MET A 818
      ...
TER    8545      ALA B 191
MASTER      517    0    0   50   28    0    0    6 8541    4    4  112
END
```

Fig. 3. Extract from PDB file 6m71.pdb describing a tetranucleosome (http://www.rcsb.org/pdb/files/6m71.pdb).

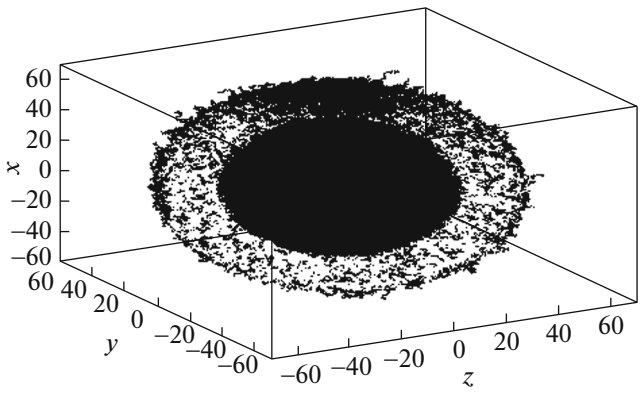

Fig. 4. 3D Track structure of SARS CoV-2.

I: potentiel moyen dexcitation,
$\beta^2 = 1 - \frac{1}{\gamma^2}$ with $\gamma = \frac{E}{mc^2}$,
δ: density effect correction factor,
$F \pm (\tau, \tau_{up})$: Function based on the Möller cross section where $\tau = \gamma - 1$ and $\tau_{up} = \min(\tau_c, \tau_{\max})$ with $\tau_c = \frac{T_{\text{cut}}}{m_e c^2}$ and $\tau_{\max} = \frac{\tau}{2}$ maximum transferable energy during the collision.

2.2.2. Secondary electrons. The production of secondary electrons with an energy higher than the production threshold T_{cut} is simulated discretely. The total effective cross section of production is calculated by integration of the differential effective cross section:

$$\sigma(Z, E, T) = \int_{T_{\text{cut}}}^{T_{\max}} \frac{d\sigma(Z, E, T)}{dT} \mathrm{d}T. \qquad (2)$$

When the incident electron irradiates inside COVID-19, a series of collision processes occur between the energetic electrons and the structural molecule of the virus. Based on the energy loss situation, this collision process can be divided into an elastic diffusion process without energy loss and an inelastic diffusion process with energy loss [12]. In the present study, we compute the elastic scattering process with the Rutherford mode, and we manage the inelastic scattering process with the fast secondary electron (FSE) mode. Each electron (including the incident electron and the generated secondary electron) must be tracked. electron) until its energy is depleted or it exits the surface of the COVID-19 through a numerical Monte Carlo simulation. The elastic scattering process requires that a scattering angle be obtained when the electron collides with the atoms. Here, the Rutherford model was used to calculate the elastic scattering cross section σ_E:

$$\sigma_E = 5.21 \times 10^{-21} \frac{z^2}{E^2} \frac{4\pi}{\alpha(1+\alpha)} \left(\frac{E + 511}{E + 1022} \right)^2. \qquad (3)$$

Here, E is the electron energy, z is the atomic number, is the shielding factor which indicates the shielding capacity of the outer electron on the nucleus. For COVID-19 which is a polyatomic molecule, the atomic number can be treated as an average atomic number. With respect to the inelastic scattering process, we must take into account not only the angle change but also the energy transfer [13]. On the basis of the FSE mode, this inelastic scattering cross-section σ_{in} can be designated as follows when it is taken as a quantum rotation mode:

$$\sigma_{\text{in}} = \int_{\Omega_c}^{0.5} \left(\frac{d\sigma}{d\Omega} \right)_M$$

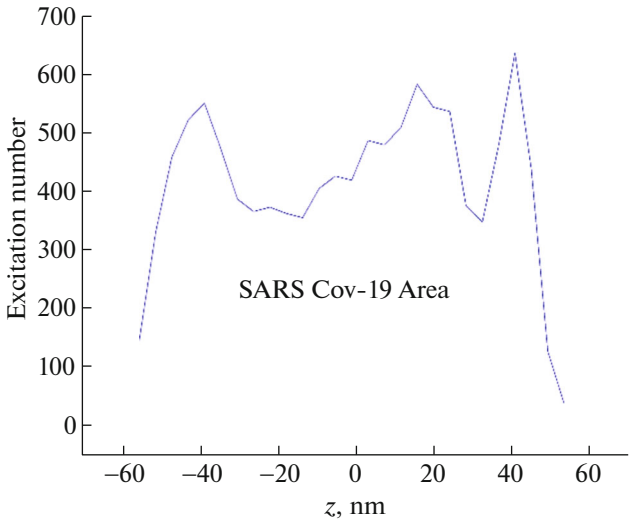

Fig. 5. The excitation number distribution according to the z-direction.

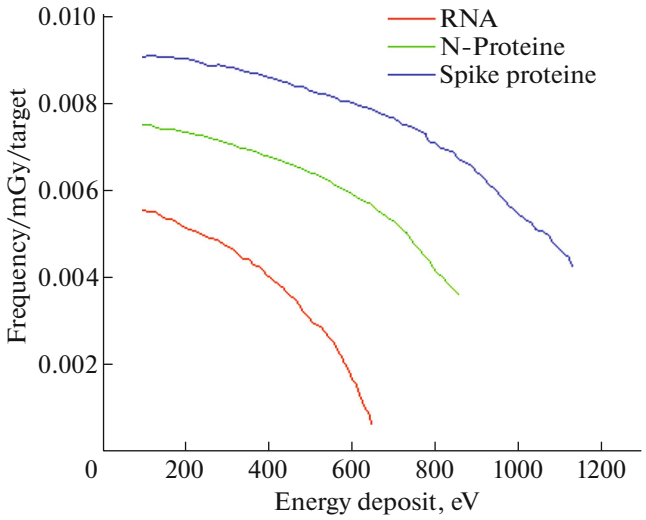

Fig. 6. The frequencies of energy deposition in Spike-protein, N-protein, and RNA.

$$= \frac{\pi e^4}{E^2} \left\{ \frac{1}{\Omega_c} - \frac{1}{1 - \Omega_c} + \ln\left(\frac{\Omega_c}{1 - \Omega_c}\right) \right\} \qquad (4)$$

with Ω_c is the lower limit of normalized energy loss coeficient.

The deposited energy is recorded in concentric layers whose thickness is a fraction of the CSDA (Continuous Slowing Down Approximation) path of the primary electrons. The calculation of the dose kernel point (normalized and dimensionless quantity) is carried out according to the following formula [14]

$$J(r/R_{\text{CSDA}}, E) = 4\pi r^2 D(r, E) \frac{R_{\text{CSDA}}}{E} \qquad (5)$$

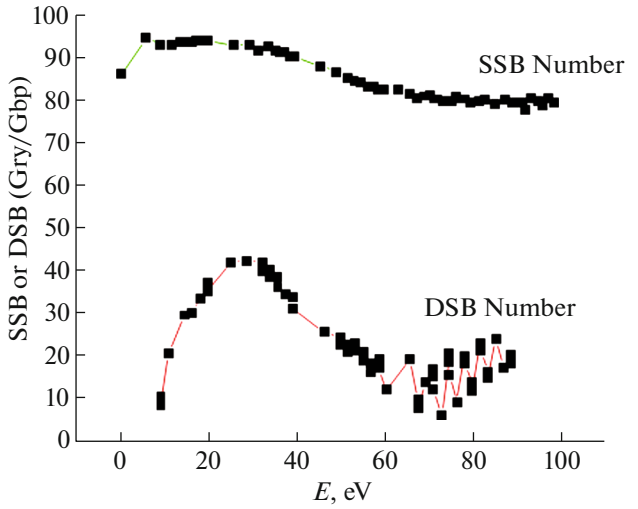

Fig. 7. The frequencies of energy deposition in Spike-protein, N-protein, and RNA.

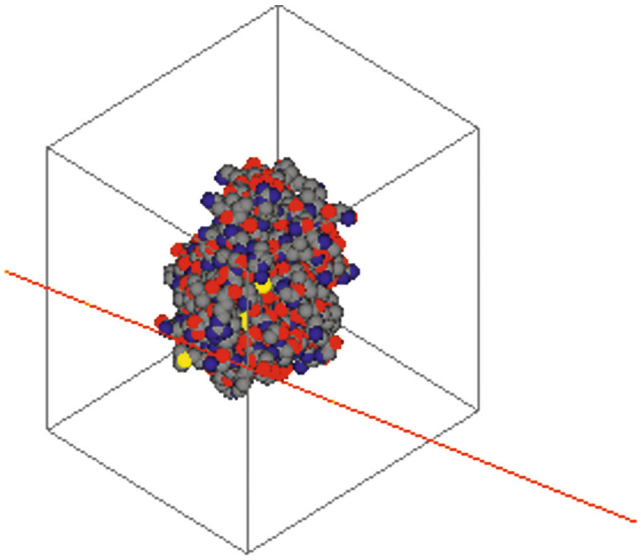

Fig. 8. Atomistic visualization with Van der Waals radius of RNA.

$J(r/R_{\mathrm{CSDA}}, E)$ is the normalized quantity representing the share of energy deposited by primary particles in a spherical layer delimited by the rays r/R_{CSDA} and $r/R_{\mathrm{CSDA}} + d(r/R_{\mathrm{CSDA}})$.

The energy loss (dE/dS) can be calculated by Bethe mode:

$$\left(\frac{dE}{dS}\right) = 78\,500\frac{\rho Z}{AE}\ln\left(\frac{1.166(E+kJ)}{J}\right) \qquad (6)$$

such as is the density of the material, Z is the atomic number, and A is the mass of the atom, k is the correction factor, J is the ionization energy, and dS is Bethe Surface. For COVID-19, Z, A, and J should be the average number of atoms, the average atomic mass, and the average ionization energy.

2.3. Monte Carlo Method

The application of the Monte Carlo method at the microscopic and nanoscopic scale is very interesting in radiobiology to calculate energy deposits in volumes of small dimensions to estimate the damage to cells and molecules [15] of DNA (single and double-stranded breaks) as well as cell survival rates. Monte Carlo simulation codes at the microscopic and nanoscopic scales are based on the so-called "trace structure" technique. Such codes provide the distribution of the coordinates in space of all interactions of the primary particle as well as the secondary particles generated. Most of the effective sections used in the Monte Carlo trace structure are calculated by a combination of data experimental and theoretical models. The theoretical models developed are to be validated with the experimental data when available. All such data must be able to describe the physical phase, i.e., the set of elemental interactions (mainly ionizations and excitations) that cause deposition of energy.

2.3.1. Geant4. Geant4 (Geometry and Tracking) is a tool for simulating the passage of particles through matter by the Monte Carlo method maintained and developed by an international collaboration. Since 1993, this tool has been developed in C++ language by a CERN Group and a CEC Group. The Geant4 simulation code was initially developed for the needs of the LHC (Large Hadron Collider) experiments and publicly distributed for the first time in 2001 [16]. Thanks to many features of Geant4, such as geometric shapes, materials, elemental particles, electromagnetic physical processes, optical and hadronics, visualization, detector sensitivity, extraction of the information from the simulation at different stages, users can build a full simulation.

2.4. Determination of DNA Breaks

2.4.1. Integration of the PDB (Protein Data Bank) file in Geant4. The PDB format. The PDB (Protein Data Bank) file format is a text file format describing the three dimensional structures of the molecules held in the Protein Data Bank. The PDB format provides for the description and annotation of proteins and nucleic acid structures. A PDB file is a text file that consists of lines of information. Each line of the file contains different types of structural information about the molecule. In Fig. 8 and Table 2, we present an excerpt from a PDB file, and the descriptions the more used [17].

For the COVID-19 simulation, it is not relevant to load the atomic representation of the PDB (Protein

DATA Bank) file via Geant4 volumes into memory. The simulations are therefore performed inside a box containing the structure of the molecule and made of liquid water. A specific algorithm makes it possible to associate the position of the energy deposits returned by Geant4–DNA to an atom of the PDB structure. To calculate the number of Single-Strand DNA Breaks (SSB), it is assumed that an energy deposit greater than in the sugar-phosphate group is sufficient to induce this break. This energy threshold corresponds to the first excitation energy level of liquid water in the physical models of Geant4–DNA. This threshold value is adjustable. To calculate the number of Double-Stranded DNA Breaks (DSB), we assume that a maximum distance of 10 base pairs between two DSB induces DSB [18]. This default setting is also adjustable.

3. RESULTS

3.1. Track Structure

Figure 3 illustrates the track structures of the volume of COVID-19. 20 000 electrons are defaulted here to better describe the ionization characteristic. The incident electrons and internal secondary electrons generated will occur through a series of inelastic ionization processes, the final amount of ionization is much greater than the number of incident electrons.

3.2. Ionization Distribution

From Fig. 4 we can intuitively obtain the ionization situation in each of the four layers. As the peak proteins are weakly distributed along with the outer envelope, the ionization experienced is not as high as in the spike-protein. The major excitation occurred in the spike-protein envelope as shown. After passing through space, the N-protein undergoes strong electron beam ionization, whereas, in the center of the COVID-19 virus, the RNA ionization rapidly withdraws with the R radius.

3.3. Calculation of Energy Deposition Frequencies

Figure 5 shows the variation in energy deposition frequencies in the Spike-protein, N-protein, and RNA layers obtained at the depth of the Bragg peak and monoenergetic electrons corresponding to the average energy of the spectrum at the same depth of the E-beam line spectrum.

3.4. RNA Damage Determination

Figure 6 shows the number of single or double-strand breaks calculated for twelve RNA base pairs (6m71.pdb file) after electron irradiation. monoenergetic from 10 eV to 50 keV. These two figures show us that the number of single or double-stranded RNA breaks is maximum at 100 eV.

4. DISCUSSION AND CONCLUSION

In this paper, we studied the properties and results of the interaction of the radioactive electron beam with the physical model of COVID-19 tuned by the Protein Data Bank using Monte Carlo numerical simulation. After modeling the molecular structure and dispersion processes of COVID-19, we obtained the following results.

The main ionization damage occurs in the protein layer of the envelope to protect the RNA.

The energy loss of the electrons interacting with the COVID-19 atoms is concentrated on 10 to 100 eV at 90%.

Physical DNA models from Geant4, which were used to study the frequency of energy deposition in COVID-19 RNA, showed that the number of single or double-stranded RNA strand breaks is at most 100 eV.

Our calculations of DNA molecule strand breaks are still limited because the Physico-chemical and chemical steps play an important role in the production of DNA damage. These models are under development and the Geant4 example we have developed will need to be adapted.

ACKNOWLEDGMENTS

The authors would like to thank the engineer Yassin Badri who provided information and expertise that greatly contributed to the research and for his comments that helped to improve the manuscript.

REFERENCES

1. S. K. Lau, P. C. Woo, C. C. Yip, H. Tse, H.-W. Tsoi, V. C. Cheng, P. Lee, B. S. Tang, C. H. Cheung, R. A. Lee, et al., Journal of Clinical Microbiology **44**, 2063 (2006).
2. J. A. Al-Tawfiq, A. Zumla, and Z. A. Memish, Travel Medicine and Infectious Disease **12**, 422 (2014).
3. D. S. Hui, E. I. Azhar, T. A. Madani, F. Ntoumi, R. Kock, O. Dar, G. Ippolito, T. D. Mchugh, Z. A. Memish, C. Drosten, et al., International Journal of Infectious Diseases **91**, 264 (2020).
4. A. Nevelsky, E. Borzov, S. Daniel, and R. Bar-Deroma, Journal of Applied Clinical Medical Physics **18**, 62 (2017).
5. A. Bardane, J. Tajmouaati, and A. Maghnouj, Moscow University Physics Bulletin **75**, 58 (2020).
6. Y. Du, L. Tu, P. Zhu, M. Mu, R. Wang, P. Yang, X. Wang, C. Hu, R. Ping, P. Hu, et al., American Journal of Respiratory and Critical Care Medicine **201**, 1372 (2020).
7. Y. S. Malik, S. Sircar, S. Bhat, K. Sharun, K. Dhama, M. Dadar, R. Tiwari, and W. Chaicumpa, Veterinary Quarterly **40**, 68 (2020).

8. G. Feng, L. Liu, W. Cui, and F. Wang, Chinese Physics B **29**, 048703 (2020).
9. J. Bhola, V. R. Venkateswaran, and M. Koul, medRxiv (2020).
10. C. Chang, C. Tang, and J. Wu, Physical Review Letters **110**, 064802 (2013).
11. R. N. Kirchdoerfer and A. B. Ward, Nature Communications **10**, 1 (2019).
12. A. V. Ivantchenko, V. N. Ivanchenko, J.-M. Q. Molina, and S. L. Incerti, International Journal of Radiation Biology **88**, 171 (2012).
13. A. Bardane, J. Tajmouaati, and A. Maghnouj, Moscow University Physics Bulletin **75**, 58 (2019).
14. Z.-B. Chen, The European Physical Journal D **72**, 67 (2018).
15. A. Bardane, J. Tajmouaati, A. Maghnouj, A. Dadouch, A. Mribah, A. El Hajami, and A. Didi, Moscow University Physics Bulletin **74**, 669 (2019).
16. R. Tsang, A. Piepke, D. J. Auty, B. Cleveland, S. Delaquis, T. Didberidze, R. MacLellan, Y. Meng, O. Nusair, and T. Tolba, Nuclear Instruments and Methods in Physics Research Section A: Accelerators, Spectrometers, Detectors, and Associated Equipment **935**, 75 (2019).
17. Y. Gao, L. Yan, Y. Huang, F. Liu, L. Cao, T. Wang, Q. Wang, Z. Lou, and Z. Rao, RSCB PDB (2020).
18. W. Ma, C. Gu, L. Ma, C. Fan, C. Zhang, Y. Sun, C. Li, and G. Yang, Science China Life Sciences **1** (10) (2020).